Supplementary Information

I. Supplementary Figures

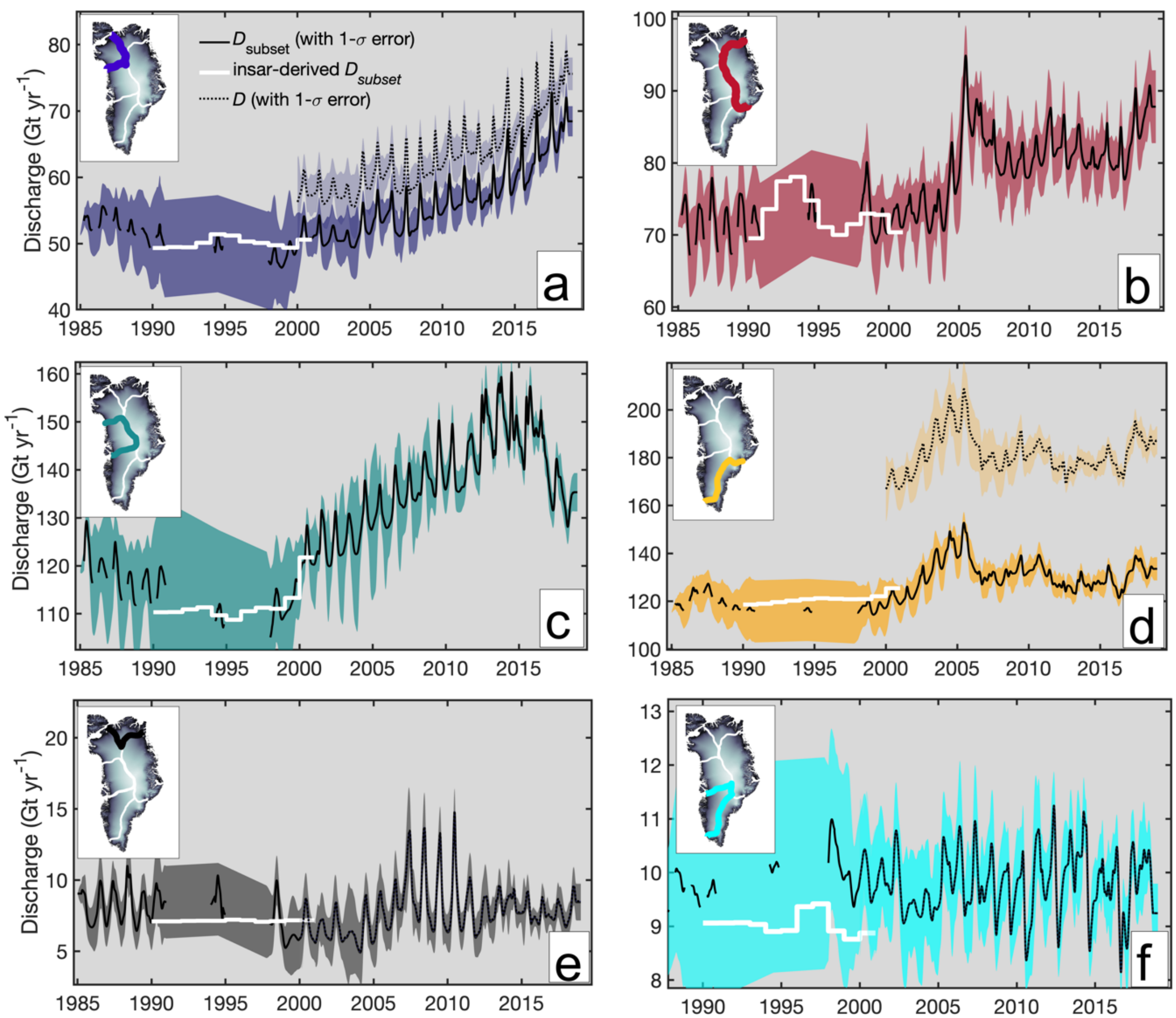

Supplementary Figure 1 | Net regional discharge times series. Time series of net ice discharge for 4 major drainage basins (NW [**a**], CE [**b**] CW [**c**], and SE [**d**]) along with the (N [**e**]) and southwest (SW [**f**]). Net regional D_t (excluding glaciers without data in 1985) is plotted by the solid black line with 1-sigma uncertainty. In the NW and SE, we also show net *D* (all glaciers including those lacking data prior to 2000) from 2000-2018. Only small, low-contributing glaciers were excluded from *D* in the CW and CE and thus only the regional total from subsetted *D*, being visibly indistinguishable from total *D*, is plotted. We also include regional totals for the northern regions (**e**), and the southwest region (**f**) although very few glaciers are included in these samples ($n < 7$). Annual *D* calculated using InSAR velocities from Mouginot et al. (2019) are shown in white for all basins during 1990-2000.

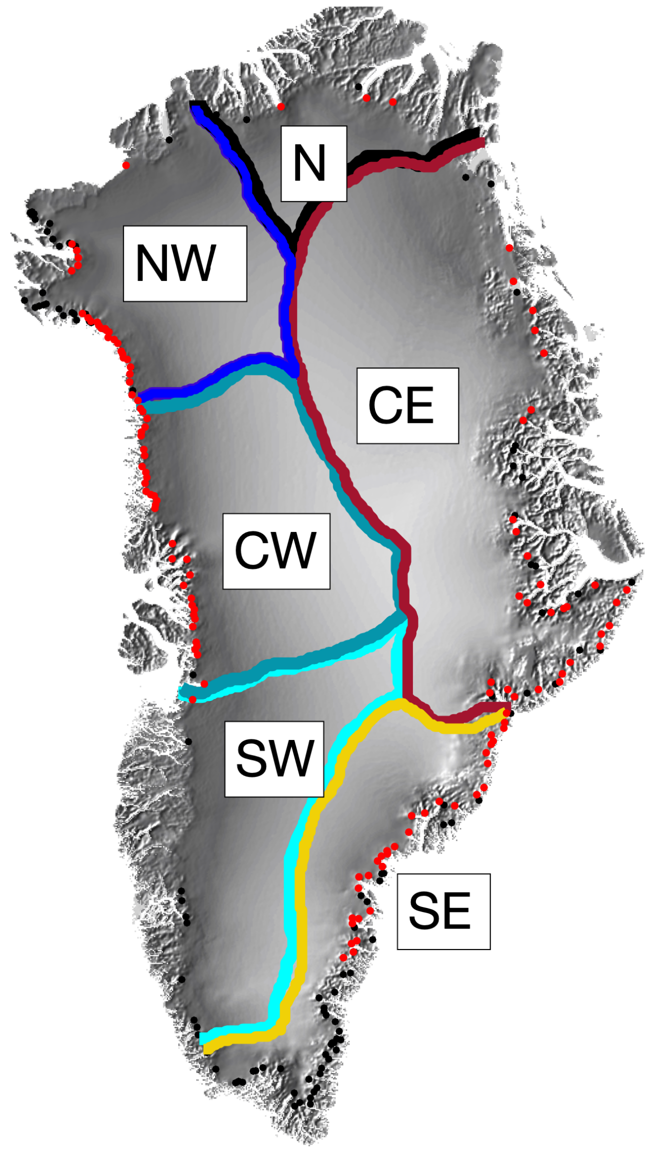

Supplementary Figure 2 | Region delineations and glacier locations. Region map showing basin delineations for the six major basins as applied in this study, including the four main drainage basins in the analysis: the northwest (NW), central west (CW), central east (CE) and southeast (SE), along with the north (N) and southwest (SW). Approximate flux gate locations of individual glaciers are marked in red and black, with red indicating a glacier where data was available for the full 1985-2018 time period.

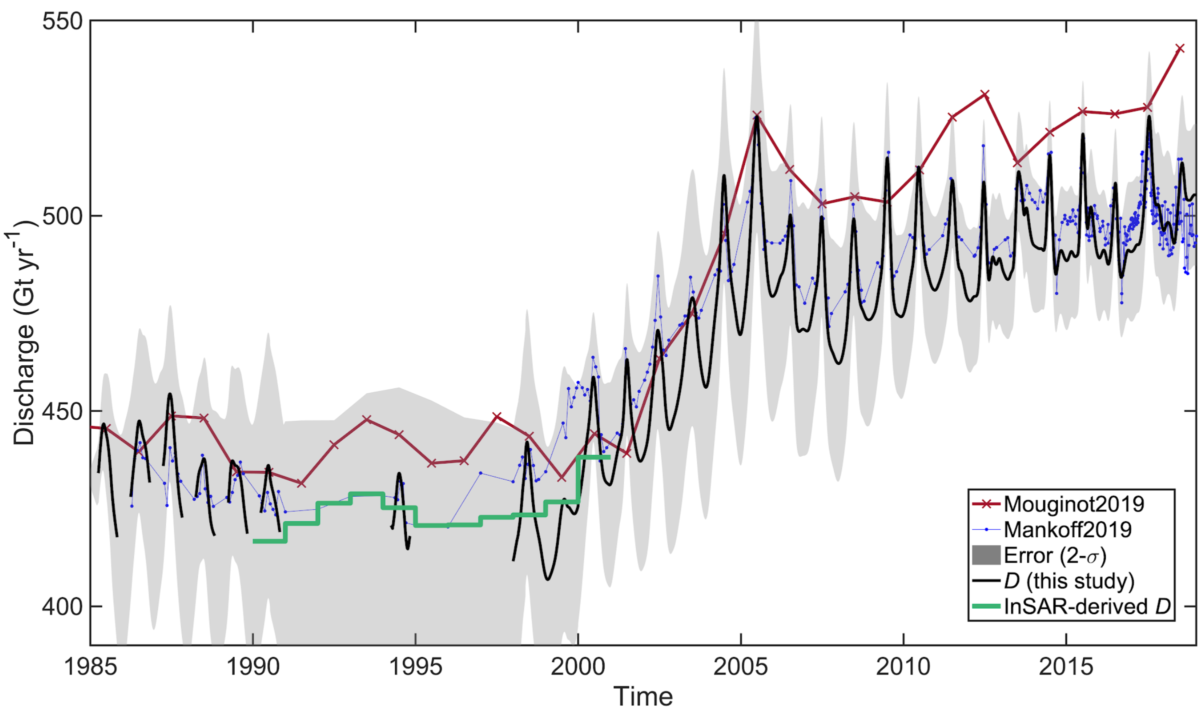

Supplementary Figure 3 | Interstudy comparison of GrIS-wide discharge estimates. GrIS discharge estimates from this study (black), compared with those from Mouginot et al., 2019 with ice caps removed (burgundy), and Mankoff et al., 2019 (blue). Annual *D* independently calculated from InSAR velocities from Mouginot et al. (2019) are shown in green.

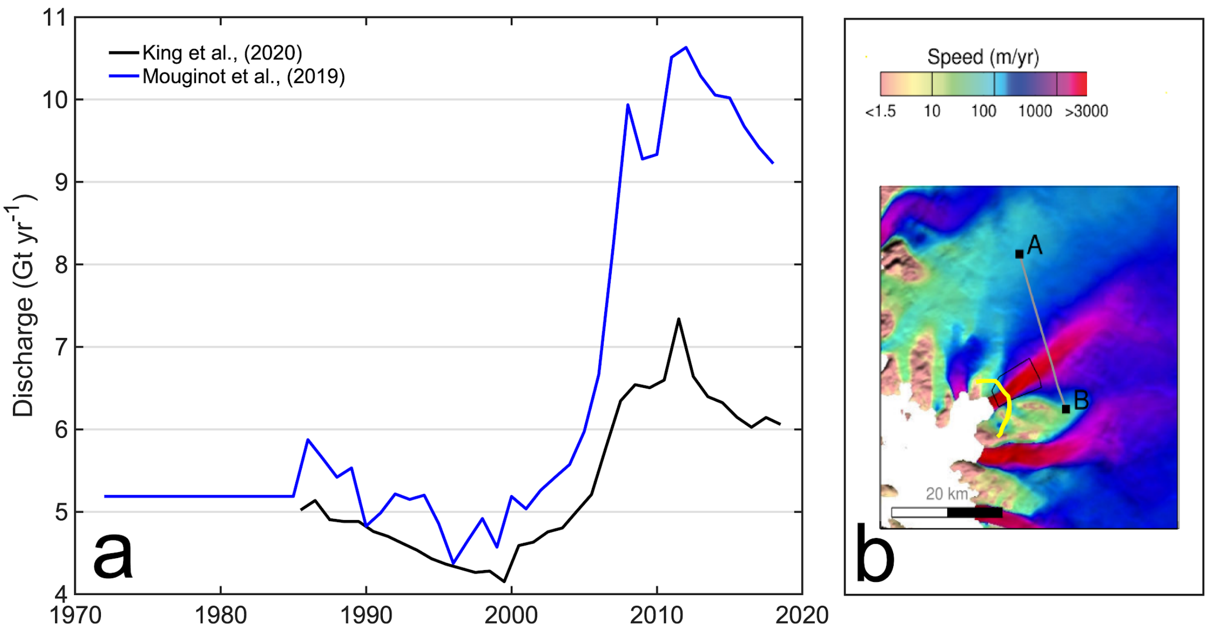

Supplementary Figure 4 | Glacier-scale example of large interstudy divergence in discharge estimates. (**a**) Annual discharge comparisons between Mouginot et al. (2019), in blue, and this study (black) at Upernavik North glacier. (**b**) Insert of Supplementary figure from Mouginot et al. (2019), showing their flux gate (between points A and B) and the region where velocities, used to scale discharge through the flux gate through time, were extracted (region outlined in black). The approximate location of the flux gate used in this study is plotted near the front, in yellow.

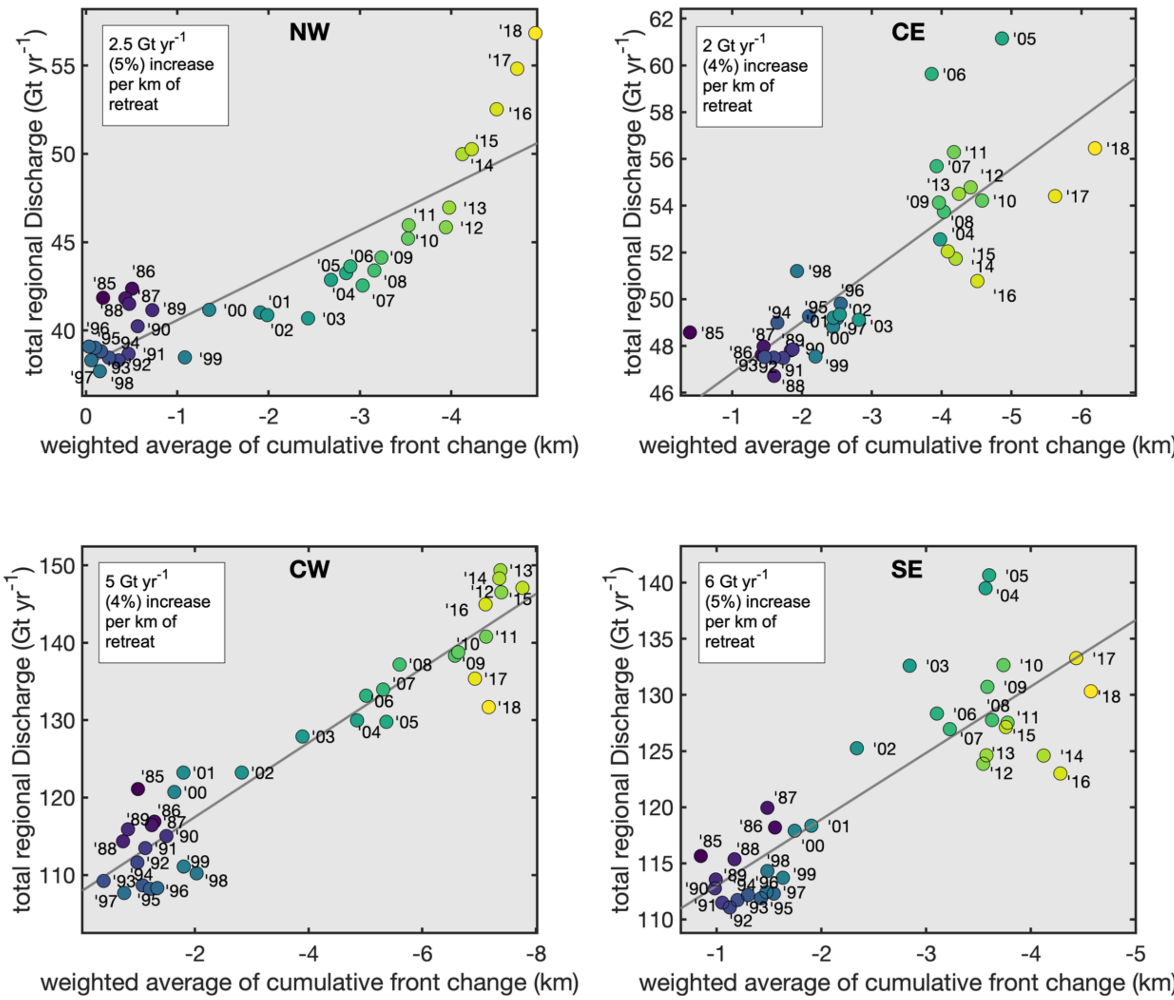

Supplementary Figure 5 | Regional relationships between discharge and front position. Annual total *D* versus net front position change for each of the four major drainage basins. Colored markers correspond to the year of observation beginning in 1985 (indigo) through 2018 (yellow). Negative front change indicates net retreat from the glacier fronts' initial position over the calendar year.

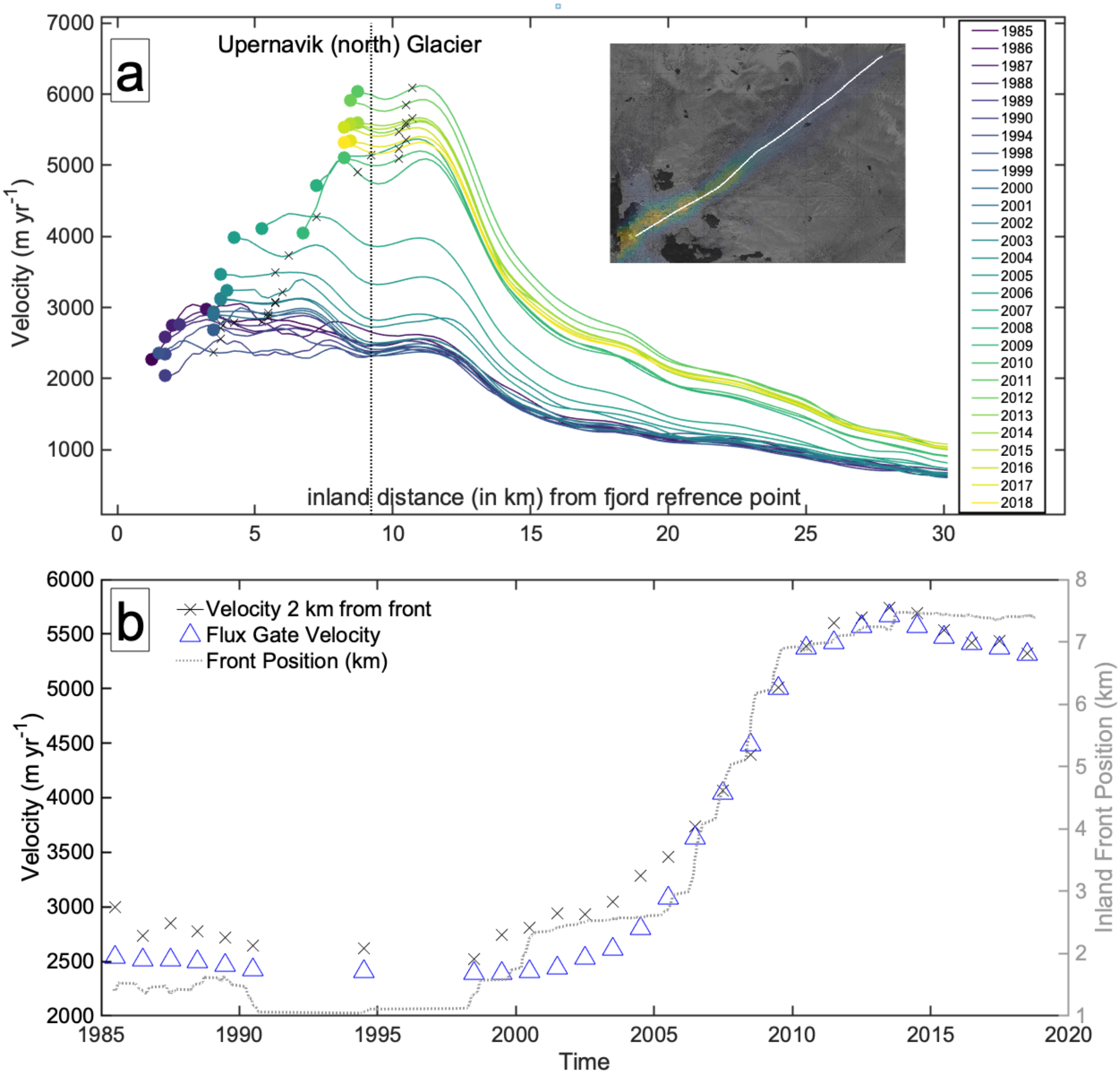

Supplementary Figure 6 | Sensitivity of velocity vs. front change relationship to flux gate position. (**a**) Average annual along-flow velocity at Upernavik North Glacier through time, plotted from the front to a fixed inland up glacier. Black x's mark the point 2 km inland from the front, and the vertical dotted line marks the static flux gate position. (**b**) Annual velocities at the flux gate and 2 km from the front (left axis) vs. cumulative front position change (right axis).

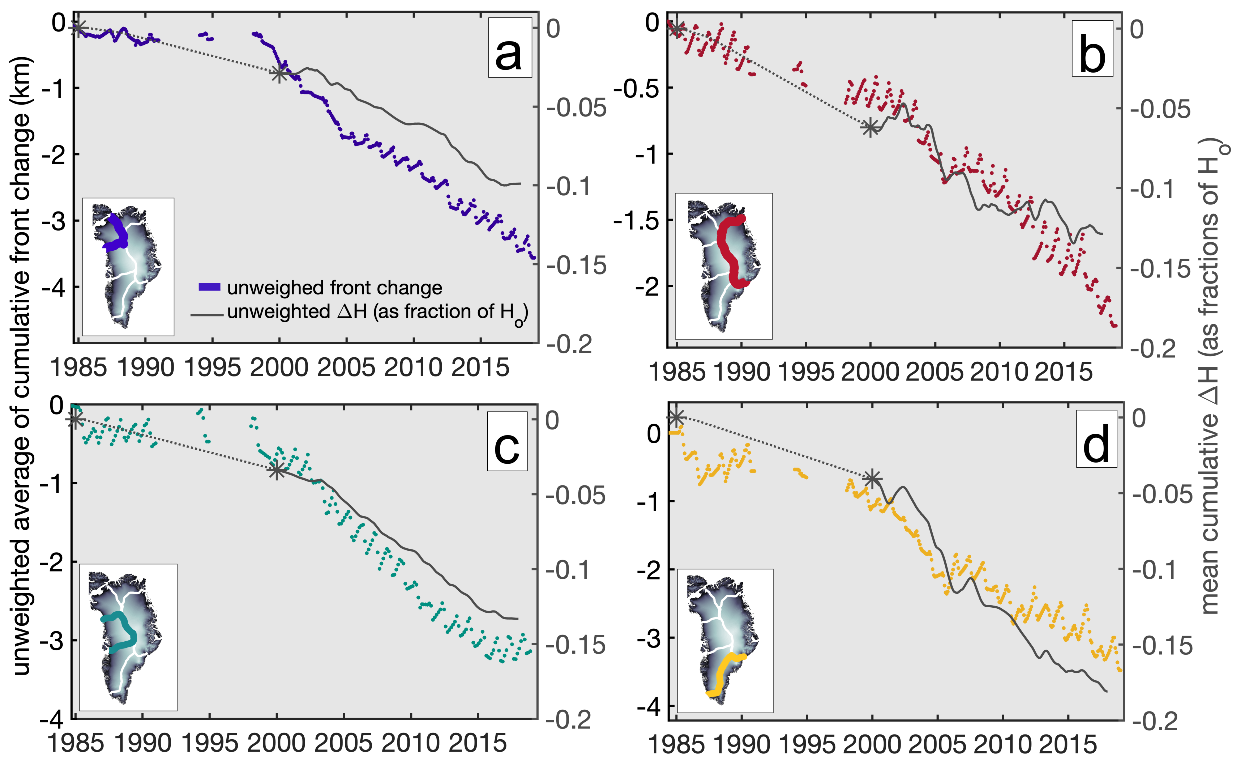

Supplementary Figure 7 | Mean unweighted regional trends in ice thickness and front position. Mean regional trends in (black curves) ice thickness and (colored curves) front position, for the northwest (**a**) central east (**b**), central west (**c**) and southeast (**d**), with the colors corresponding to the locations mapped in the left plane. Negative values on the left y-axis indicate net cumulative retreat over the study period. Cumulative thickness change is calculated from the mean of all regional glaciers and expressed as fractional changes from H_o. Lighter, dotted gray lines between the two starred points indicate linear interpolation between two sparse data points, and the apparent trend during this period should be treated with caution. Please note that the limits along the left y-axes vary between panels so that time series details are more visible.

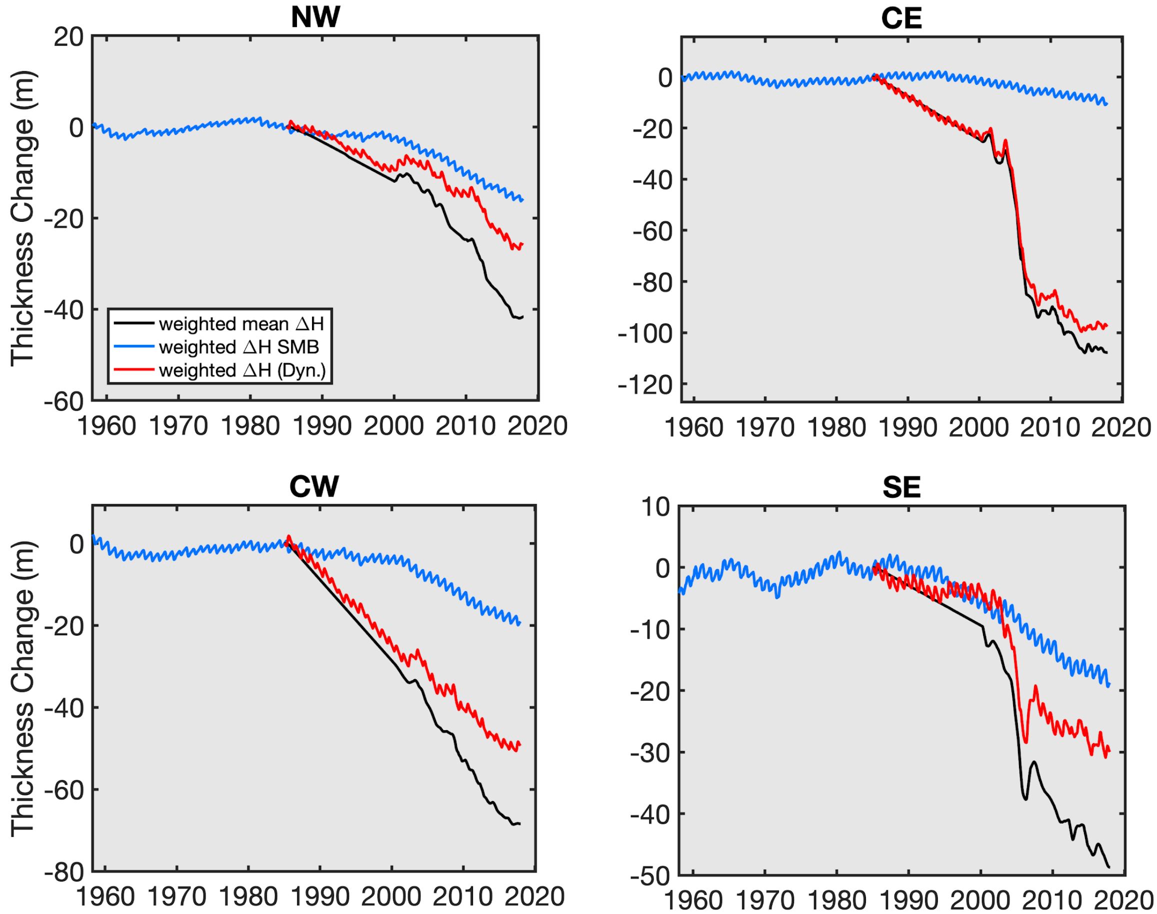

Supplementary Figure 8 | SMB and dynamic components of cumulative regional ice thickness changes. Changes in weighted cumulative ice thickness anomalies relative to the 1961-1990 reference period for each of the four major basins, with anomalies accruing beginning in 1985. Means are calculated from time series weighted by individual glacier flux and are broken into SMB (blue) and dynamic (red) components.

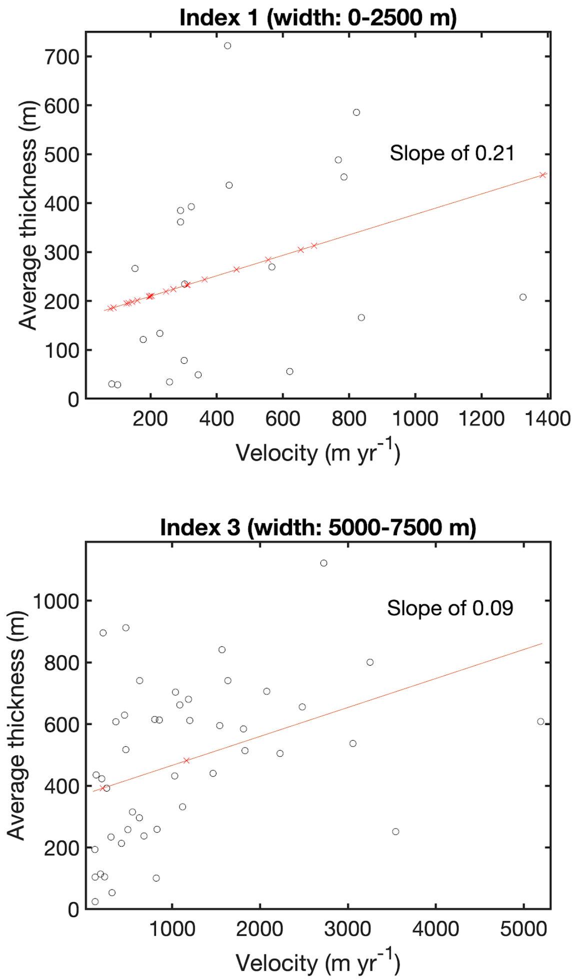

Supplementary Figure 9 | Bed topography adjustments from velocity-thickness relationships. Best fit between centerline velocity and ice thickness calculated from valid glaciers (black markers) for four subgroups, binned based on terminus width. Invalid ice thicknesses adjusted based on each fit are plotted by red x's.

II. Supplementary Discussion

We attribute this divergence between our and Mankoff et al. (2019) net discharge values with those in Mouginot et al. (2019) after 2002 (Supplementary Figure 4) to the use of reference fluxes in Mouginot et al. (2019), as well as the treatment of how thinning impacts *D* through time. Mouginot et al. (2019) calculates *D* from glaciers with missing or problematic bed topography by assuming a reference ice flux equal to the surface mass balance of the basin (i.e., the glacier is assumed in balance at the beginning of the time series), whereas this study does not make any reference flux assumptions and calculates *D* directly using bias-corrected ice thicknesses, where needed. Without integrating an ice thickness term, discharge calculated from glaciers using SMB-referenced fluxes in Mouginot et al. (2019), which total ~80 Gt yr^{-1}, can therefore only be scaled by changes in velocity through time but do not take into account reductions in *D* from thinning. Assuming this subset of glaciers thin at similar rates to those with reliable bed topography, we would expect thinning to impart a 10% decrease in *D* over the time period, or ~8 Gt by 2017. While this value is small and within errors of available ice thickness and scaling methods, it explains about 20% of the interstudy divergence.

Mouginot et al. (2019) also use an areally averaged velocity to scale *D* through time, rather than directly extracting velocity along discrete flux gate coordinates as done here. At some glacier basins, this average is computed from over a region fully in front of the gate, and thus may overestimate proportional changes in velocity, used to scale *D*, at the inland gate location where thickness changes are measured. Indeed, at the individual glacier-scale, our results deviate the most from their estimates at these such sites (an example shown in Supplementary Figure 4 at Upernavik North Glacier). Methodological differences in estimating glacier thinning and its impact on *D* through time is therefore the likely source of discrepancy in both absolute discharge values and long-term trends between the two studies.

III. Supplementary Methods

Sensitivity of velocity vs. front position relationship to flux gate position

We aggregate mean annual front changes and velocity along a flowline for the 15 fastest-flowing glaciers in our sample. We then derive linear relationships between cumulative front position and velocity 2 km from the time-dependent front positions. We find significant correlations ($p < 0.05$) at 11 of the 15 fastest flowing glaciers, with 9 of the 11 yielding significant positive correlations. The four glaciers lacking a significant correlation between 2 km velocity and cumulative front position are either positioned on prograde beds or have a near-static front position (cumulative change < 1 km). This suggests that the timing and magnitude of front-induced changes in discharge are insensitive to whether static or fixed-distance velocities are tested because retreat is associated with nearly instantaneous acceleration well inland of our fixed gates. An example of this is shown in Supplementary Figure 6.

Supplementary References

1. Mankoff, K. D., Colgan, W., Solgaard, A., Karlsson, N. B., Ahlstrøm, A. P., van As, D., Box, J. E., Khan, S. A., Kjeldsen, K. K., Mouginot, J., and Fausto, R. S. Greenland Ice Sheet solid ice discharge from 1986 through 2017, *Earth Syst. Sci. Data*, **11**, 769–786, (2019).
2. Mouginot, J., Rignot, E., Bjørk, A. A., van den Broeke, M., Millan, R., Morlighem, M., Noël, B., Scheuchl, B. and Wood, M. Forty-six years of Greenland Ice Sheet mass balance from 1972 to 2018, *Proc. Natl. Acad. Sci.*, **116**, 9239–9244, (2019).